Design and test of the anti-skid system for self-propelled high-stem crop sprayers

Haojun Wen[1,2], Xinyue Liu[1*], Zhetian Yi[1], Zhongxiang Li[1]

(1. *School of Mechanical and Electrical Engineering, Shihezi University, Shihezi 832003, Xinjiang, China*;
2. *Northwest Key Laboratory of Agricultural Equipment, Ministry of Agriculture and Rural Affairs, Shihezi 832003, Xinjiang, China*)

Abstract: Aiming at the problem of skidding in the operation of a self-propelled high-stem crop sprayer due to uneven road surface and uneven distribution of soil cohesive force, This study proposed a four-wheel drive hydraulic anti-skid control system based on RTM valve. Through theoretical analysis of control components such as the RTM valve and steering cylinder, the control model of the anti-skid drive system of the spray machine was established, and the simulation test was carried out in Matlab/Simulink. The simulation results show that the slip rate of the anti-skid drive system based on the PID control strategy is controlled below 0.05, and the RTM valve keeps the driving pressure of the system basically stable. In order to verify the reliability of the simulation results, the designed drive anti-skid control system was carried out on a spray machine for the field test. The experimental results show that the slip rate of the drive anti-skid system decreases from 86.7% to 1.25% when the anti-skid function is turned on, indicating that the designed drive anti-skid system has good anti-skid performance.
Keywords: self-propelled sprayer, high-stem crops, drive anti-skid, PID control, Matlab, Simulink
DOI: 10.25165/j.ijabe.20231606.5825

1   Introduction

With the rapid development of agricultural machinery, self-propelled high-stem crop sprayers have gradually become an important tool for the disease and insect pest control of cotton, maize, rice, and other crops in the middle and late period due to its advantages of a wide spraying range, good atomization effect, and strong drug permeability. Compared with the traditional traction sprayer, the large turning radius and small ground clearance lead to crop damage and harvest impact. The self-propelled high-stem crop sprayer has the obvious advantages of full hydraulic drive[1-3], higher operating efficiency, and higher flexibility.

However, Once the driving wheel of the vehicle has a skidding phenomenon, affecting the stability of the vehicle. Zhang et al.[4], put forward a driving force coordination control strategy with road identification for eight wheeled electric vehicles, and a controller based on sliding mode control with a conditional integrator uses this value for acceleration slip regulation; Guo et al.[5], put forward a MPCA method is proposed to reasonably distribute the virtual input among four in-wheel motors in order to optimize the tire slip power loss and vehicle stability performance; Fukui et al.[6], respectively proposed corresponding theoretical control strategies for vehicle skid swing with different wheels, such as *X* drive layout and *Z* drive layout of four-wheel drive vehicles, and verified their proposed control strategies using an equal-scale test bench; Chen et al.[7]

analyzed wheel-rail rolling contact characteristics of heavy-haul locomotive under complex wheel-rail friction conditions, systematically compared and analyzed the influence of different anti-slip control models on wheel-rail adhesion utilization of locomotive.

At this stage, anti-slip control is widely used in highway traffic and rail transit, and it is also integrated into some high-end agricultural machinery abroad, but it is still relatively rare in proportion. There has been a deep accumulation of theoretical research on anti-skid control in China, but it is more concentrated on traditional mechanical vehicles such as automobiles and trains, and less research on agricultural machinery, especially hydraulic driven agricultural machinery.

The hydraulic oil of the hydraulic drive system always flows from high-pressure area to low-pressure area. the pressure located in the driving shaft will drop to the system's low pressure, and the system flow will converge to the driving shaft, resulting in the driving wheel turning faster, therefore, this study designed a drive anti-skid control system based on an RTM valve (The RTM valve is a flow divider for controlling hydraulic motors ensuring synchronous and free-wheel operation. It can have multiple drives available upon request. It can be operated in open and closed circuits) and PID control, the control model was established and simulated, and the anti-slip effect of the control system was verified by field experiment.

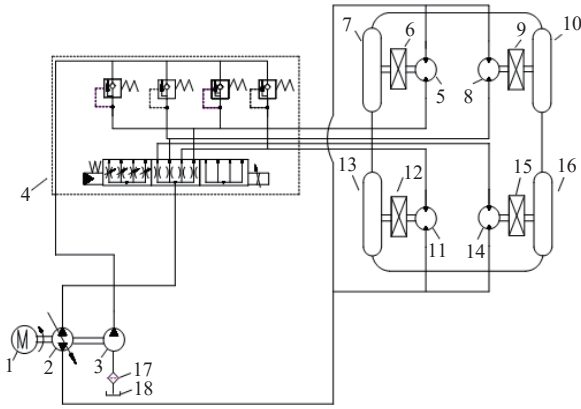## 2   Anti-skid control system design principle

2.1   Overall drive layout design

A single hydraulic pump drives four hydraulic motors through the RTM valve, and the hydraulic oil flowing from the pump passes through the RTM valve and is evenly distributed across the four hydraulic motors as shown in Figure 1, thus preventing hydraulic oil from flowing to the motor as the wheels slip, exacerbating the slip phenomenon. The solution has the characteristics of simple system structure, low costs, and good anti-slip effects.

1. Engine 2. Main oil pump 3. Auxiliary oil pump 4. Non-skid control valve 5. Left front motor 6. Left front accelerator 7. Left front wheel 8. Right front motor 9. Right front reducer 10. Right front wheel 11. Left rear motor 12. Left rear reducer 13. Left rear wheel 14. Rear right motor 15. Rear right reducer 16. Rear right wheel 17. Filter 18. Hydraulic oil tank

Figure 1   Single RTM valve control scheme and requires high system cooling

However, because the flow loss is large when hydraulic oil flows through the damping holes in the RTM valve, the system consumes more energy and heat in order to reduce the energy loss of the system, the two-way valve integrated into the RTM valve can be opened when the surface attachment conditions are good. When the wheels do not slip, the solenoid valve is powered off and the hydraulic oil can flow freely. When the wheels slip, the solenoid valve can be opened to force the modulation of hydraulic flow that does not reach each tire for non-slip control[8-10]. In addition, anti-skid control can be realized to make the vehicle turn with small deflection angle. Set a fixed throttle between the two branches of the collection valve so that the oil in the two branches is connected by a hole as it rotates (there is a pressure difference on both sides of the hole and the flow is very small)[11,12]. There may be a speed difference between the two hydraulic motors during steering, by changing the motor displacement through weak current control, the differential control and differential anti-slip control are realized[13,14]. For ease of discussion, the sprayer drive wheel number is shown in Figure 2.
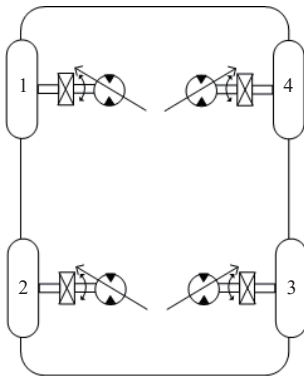
1. Left front wheel 2. Right front wheel 3. Left rear wheel 4. Right rear wheel

Figure 2   Wheel number marking drawing

2.2   Calculation of slip rate

If the sliding rate of a wheel with a low speed is s_0, the speed calculation equation is the sliding rate of the lowest wheel and its speed is calculated as:

$$\omega_1 = \frac{v}{r(1-s_0)} \tag{1}$$

where, ω_1 is the speed of the lowest speed wheel, rad/s; v is the vehicle speed, m/s; r is the tyre radius, rad/s.

The minimum speed wheels as the reference, the relative slip ratio of each wheel is s_r as[11]:

$$s_r = \frac{\omega_i - \omega_1}{\omega_i} \ (i = 2, 3, 4) \tag{2}$$

where, ω_i is the speed of the other speed wheel, rad/s.

The geometry of the sprayer can determine the wheelbase, wheelbase, and main pin offset distance of the implement, and the speed ratio of each wheel at different corners of the sprayer can be calculated. The actual speed of the four wheels is obtained in real-time through the wheel speed sensor, the actual speed ratio of each wheel is calculated according to the minimum actual speed of the wheel (set to 1), the displacement of the piston is detected by the displacement sensor installed on the steering cylinder, the theoretical steering radius of each wheel can be calculated, and the theoretical speed ratio of each wheel can be calculated using the same reference, and if the wheel is satisfied Equation (3), the wheel slips, it needs to be non-slip control[12].

$$\left| \frac{\omega_i}{\omega_1} - \frac{R_i}{R_1} \right| > 0.05 \ (i = 2, 3, 4) \tag{3}$$

where, R_i is the turning radius of the other wheel, m.

2.3   Control scheme design of the anti-skid system

The control system mainly includes three modules: input signal acquisition module, slip judgment module, and control execution module[15-17]. Among them, the input signal acquisition module mainly collects speed signals from 4-wheel motor speed sensors and displacements from 4 steering hydraulic cylinders, signals, and pressure signals from the two sub-oil systems[18-20]. The slip judgment module can determine the driving conditions of the vehicle and the skid conditions of the four wheels based on the collected revenue signals, thereby providing a basis for control decisions. The control execution module is based on the vehicle speed, Hydraulic system pressure, wheel slip conditions, and other information used to make decisions, obtain the optimal control scheme, and output control instructions to the corresponding control actuators[21,22]. When two or more wheels are found to be slipping, the controller immediately responds to the RTM valve and sends a control signal to proportionally throttle the slipping wheels. When only one wheel is slipping, the RTM valve is not controlled first, and the advantages of the four-wheel-drive of the sprayer are used to drive while monitoring the pressure of the sub-oil system pressure sensor and the motor speed sensor signal. When the system pressure or motor speed exceeds the set value range, it will send the RTM valve control signal to skid Wheels to apply controls to prevent excessive pressure or motor Overspeed[23-25], as shown in Figure 3.

2.4   Control model and mathematical model establishment

This spray machine adopts a full hydraulic drive system single pump RTM valve layout electronic control hydraulic design, there is no direct mechanical connection between the cab and chassis drive mechanism.

Mathematical modeling was carried out for the whole control scheme, and then MATLAB/Simulink was used for simulation modeling, and the accuracy of modeling was verified by comparing the collected data.

Flow equation on both sides of RTM valve:

$$q_1 = C_d W_x \sqrt{\frac{2(p_s - p_1)}{\rho}} \tag{4}$$
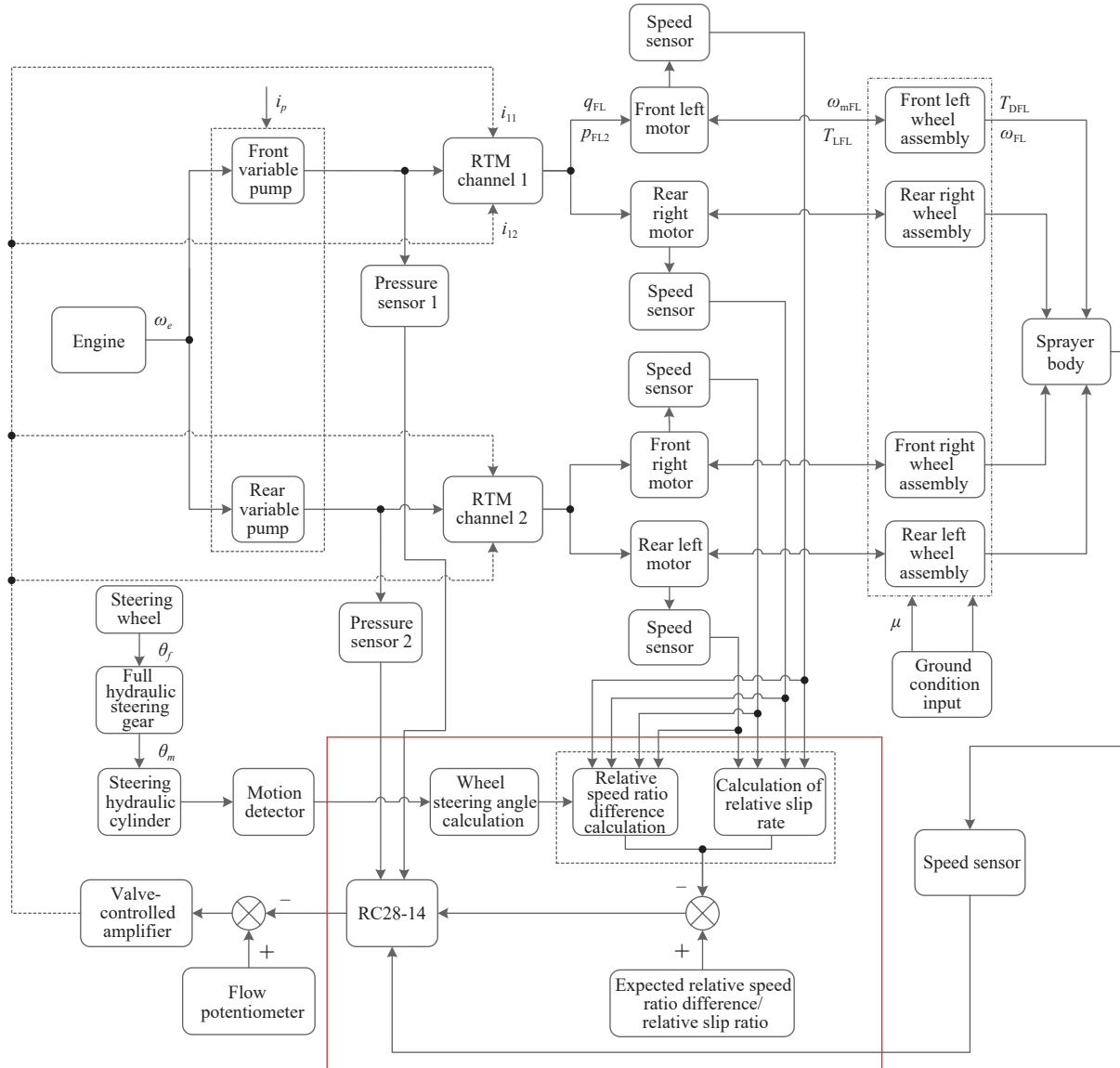
Note: The red box represents skidding judgment module; ω_e is the engine angular velocity; θ_f is the steering wheel angle; θ_m is the steering gear angle; i_p is the transmission ratio; i_{11} and i_{12} stands for input current signal; q_{FL}, p_{FL2} respectively represent the input flow and pressure of the motor; ω_{mFL} and ω_{FL} represent the input angular speed and the output angular speed of the front left wheel; T_{LFL} and T_{DFL} represent the input torque and output torque of the front left wheel; μ is the coefficient of adhesion between the tire and the ground. The red wireframe represents the skidding judgment module.

Figure 3   Block diagram of anti-skid control principle of self-propelled sprayer drive system

$$q_2 = C_d W_x \sqrt{\frac{2p_2}{\rho}} \qquad (5)$$

where, q_1 is the cylinder responds to flow, m³/s; q_2 is the cylinder block excitation flow, m³/s; ρ is the mdium oil density, kg/m³; p_1 is the in response to the pressure, Pa; p_2 is the to motivate the pressure, Pa; p_s is the input pressure, Pa; W_x is the triage area, m²; C_d is the coefficient of collector.

The load flow q_L is

$$q_L = \alpha C_d W_x \sqrt{\frac{1}{\rho}\left(p_s - \frac{x}{|x|}P_L\right)} \qquad (6)$$

where, $\alpha = \dfrac{1+n}{\sqrt{2(1+n^2)}}$, $n = \dfrac{q_2}{q_1} = \dfrac{A_2}{A_1}$, A_1 is the rodless cavity piston cross-sectional area，cm²; A_2 is the rod cavity piston cross-sectional area, cm²; x is the scalar displacement, m.

Linear processing as Equation (7).

$$q_L = K_q x - K_P P_L \qquad (7)$$

where, K_q is the steady state gain of RTM valve, m²/s; K_P is the

steady flow pressure coefficient of RTM valve, m⁵/(N·s); P_L is load pressure, Pa.

The flow continuity equation of the proportional servo valve is

$$q_L = C_{sum}P_L + \frac{V}{4\beta_e}\frac{dP_L}{dt} + A_{fir}\frac{dy}{dt} \qquad (8)$$

where, C_{sum} is the total pressure coefficient, m⁵/(N·s); V is the volume, m³; β_e is the elastic modulus of medium, N·m²; A_{fir} is the cross-sectional area of piston, m²; y is the amount of piston displacement, cm; t is the time, s.

Load equation of hydraulic cylinder:

$$P_L = \frac{my + B_p y + K_s y + F_e}{A_e} \qquad (9)$$

where, m is the load mass, kg; B_P is the viscous damping coefficient, N·s/m; K_s is the load factor, N/m; F_e is the equivalent load, N. When the cylinder block expands $F_e = F_L - \dfrac{n^2(A_1 - A_2)p_s}{1+n^2}$, when the cylinder block is compressed $F_e = F_L - \dfrac{(A_1 - A_2)p_s}{1+n^2}$, F_L is

the external load; A_e is the piston operating area, m², $A_e = \dfrac{A_1 + n^2 A_2}{1 + n^2}$.

Take the Laplace transform $Y(s)$ as follows:

$$Y(s) = \frac{\dfrac{K_q}{A_m} x - \dfrac{K_t}{A_e A_m}\left(\dfrac{V}{4\beta_e K_t} + 1\right) F_e}{\left(\dfrac{1}{\omega_h^2} + \dfrac{2\xi_h}{\omega_h} + 1\right) s} \tag{10}$$

where, A_m is the increase in air storage; K_t is the load gain factor; ω_h is the inherent frequency; ξ_h is the hydraulic power element damping ratio; s is the complex variable.

According to Equations (4)-(10), the transfer function of the anti-skid drive system $G(s)$ can be calculated as

$$G(s) = \frac{\dfrac{K_a K_b K_y}{A_m}}{s\left(\dfrac{1}{\omega_v^2} s^2 + \dfrac{2\xi_v}{\omega_v} + 1\right)\left(\dfrac{1}{\omega_h^2} s^2 + \dfrac{2\xi_h}{\omega_h} s + 1\right)} \tag{11}$$

where, K_a is the unbiased coefficient of acceleration; K_b is the gain of input current, $K_b = K_v K_q$; K_v is the velocity unbiased coefficient; K_y is the spool displacement gain coefficient; ξ_v is the servo damping coefficient; ω_v is the servo surround frequency.

To sum up, the structure diagram of the anti-skid control system is shown in Figure 4.
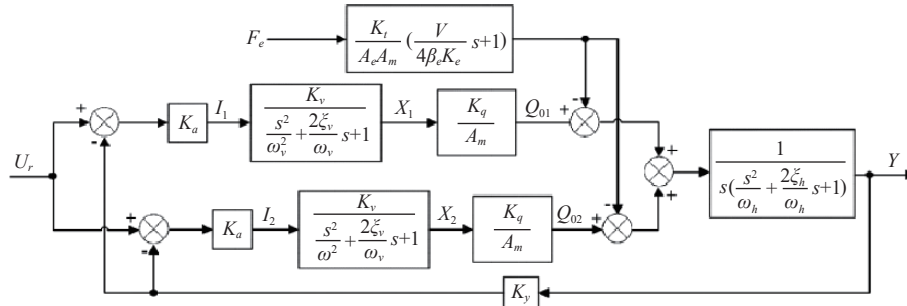
Note: U_r is the input voltage signal; I_1 and I_2 are the input current that controls the spool displacement; X_1 and X_2 are the spool displacement; Q_{01} and Q_{02} are the valve output flow.

Figure 4 Anti-skid control system simulation model structure diagram

By substituting Table 1 into the transfer Equation (11), the optimal value of K_p and K_I (K_p is the proportion coefficient, K_I is the integral coefficient) can be obtained as 52 and 0.5 after simulation calculation, and the Bode diagram is shown in Figure 5. According to Figure 5, the traversal frequency is 3.643 Hz. In the test, the interval should be between 0.1 and 5.0 Hz.

Table 1 Test platform parameter setting

Parameter name	Parameter value	Parameter name	Parameter value
Servo amplifier gain	2×10^{-3}	Cylinder block response area/m²	1.884×10^{-3}
Feedback gain	39.4090	Hydraulic cylinder has rod cavity area/m²	1.347×10^{-3}
Flow gain	8.819×10^{-3}	Hydraulic cylinder stroke/mm	203
System pressure/Pa	16	Oil bulk elastic modulus/N·m⁻²	7.8×10^8
Proportional servo valve frequency/Hz	376.8	Hydraulic natural frequency/Hz	1.96.693
Servo valve damping coefficient/N·s·m⁻¹	0.7	Hydraulic damping coefficient/N·s·m⁻¹	7.5×10^{-2}
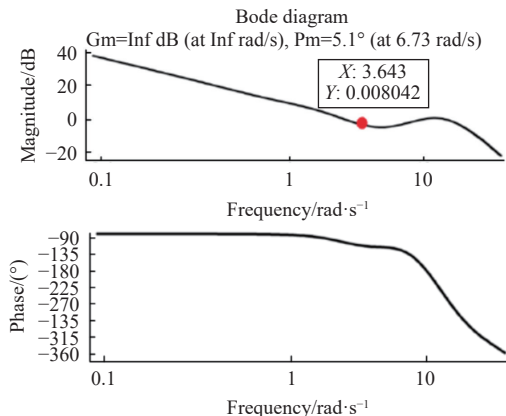
Note: Gm is the gain margin; Pm is the phase margin.

Figure 5 Bord diagram of the anti-slip control system

3 Test preparation and process

3.1 Test point layout

Twelve pressure test points are arranged in the entire chassis-driven hydraulic system (respectively placed in the main pump high-pressure ports A and B, the main pump suction port S, the main pump casing drain T port, the main pump servo control X_1 port and X_2 Port, main pump charge pressure P_s port, RTM anti-skid valve control pressure X port, left rear motor high-pressure ports A and B, left rear motor servo control X port, left rear motor casing oil discharge L port, and brake release B_r port), 5-speed test points (respectively placed at the front end of the engine crankshaft, four wheel side motor output shaft ends) and 7 temperature test points (respectively placed at the main pump suction S port, suspended and in air, and the main pump casing unloaded Oil T port, motor housing drain L port, radiator oil inlet T_1 port, radiator oil outlet T_2 port, and main pump high pressure A port), respectively, at different engine speeds, high or low speed, straight or detailed and continuous testing and recording of pressure and temperature at various test points of the system in corners, forwards or backward. The test point layout is shown in Figure 6.

3.2 Experiment procedure

Use a computer to collect the pressure, temperature, steering angle, driving speed of the drive system through the interface, and the time, duration, and number of slips when driving at various speeds on different test sections.

1) The sprayer travels at a low speed of 3 km/h in the ordinary test and slips test sections, and gradually increases the speed to 6 km/h. After the slip occurs in the slip section, the anti-skid control is turned on and the vehicle is turned After driving to the endpoint, clean the wheels and accelerate at the speed of 3 km/h on the slip road section to 6 km/h;

2) The sprayer travels at a low speed of 8 km/h in the ordinary test and slips test sections, and gradually increases the speed to 12 km/h.
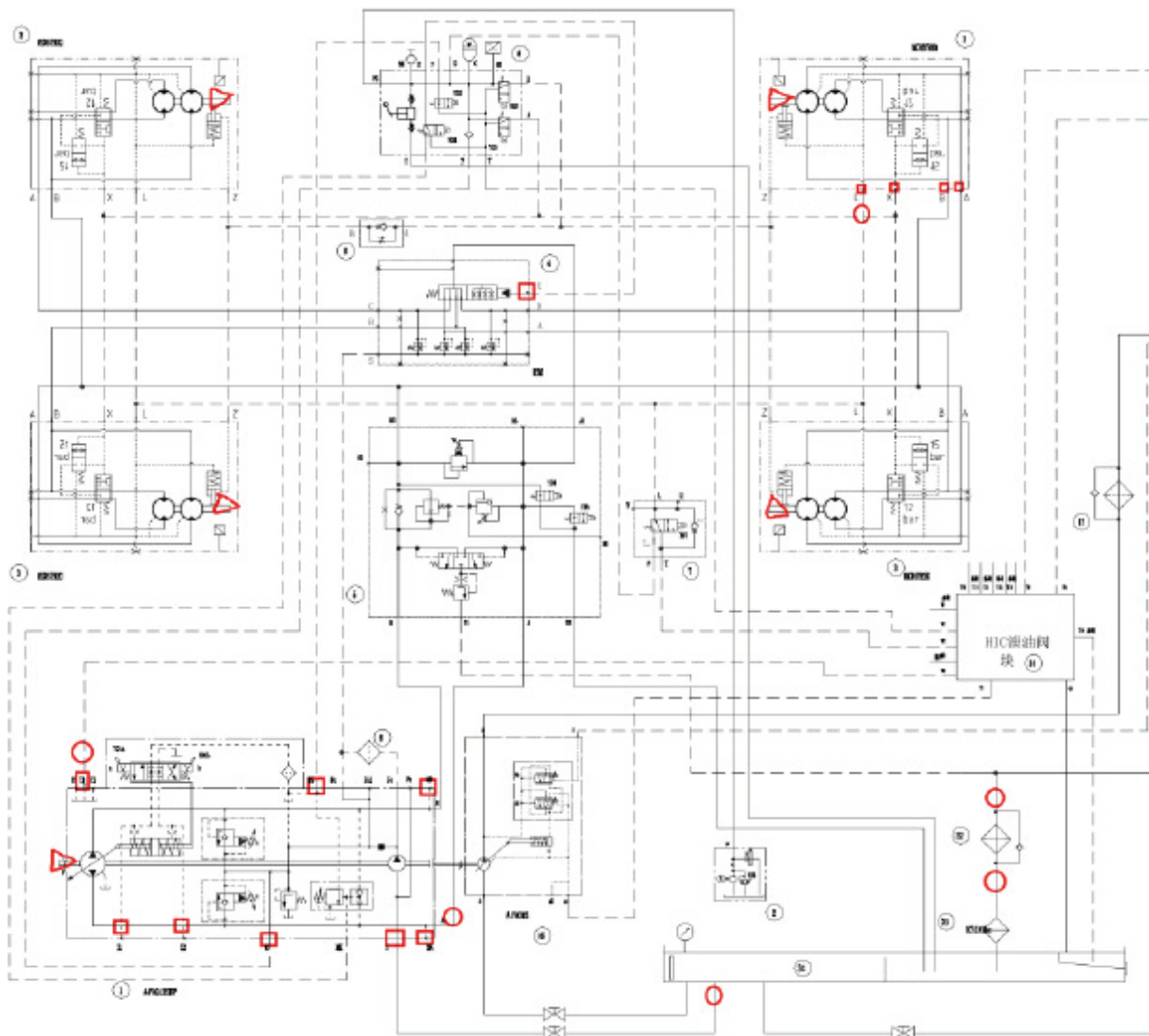
Note: The red box marks represent test pressure test point; the red triangle represents the speed test point; the red circle mark represents temperature test point.

Figure 6   Position map of self-propelled high-stem crop sprayer chassis hydraulic drive system test

After the slip occurs in the slip section, the anti-skid control is turned on and the vehicle is turned After driving to the endpoint, clean the wheels and accelerate at the speed of 8 km/h on the slip road to 12 km/h;

3) When the sprayer is turned on, the high-speed gear travels at the speed of 12 km/h in the ordinary test and slip test sections and gradually increases the speed to 15 km/h. When the slip occurs in the slip section, the anti-skid control is turned on and after the vehicle reaches the endpoint, clean the wheels and accelerate at the speed of 12 km/h on the slip road to 15 km/h;

4) After refilling the slip test section, let the sprayer turn on the anti-slip control to rotate at a high speed of 12 km/h at a 30° turn in the slip zone and gradually accelerate to 25 km/h, and then at full speed run for another 10 min.

4   Results and discussion

4.1   Low-speed group test

In the low-speed driving state of 3-6 km/h, the slip rate without the anti-skid control function is shown in Figure 7a, and certain skidding phenomenon occurs in all four wheels. It is shown in Figure 7b after the anti-skid system is started, the slip rate of the four wheels is within 0.05, the average control is around 0.027, and the highest slip rate of wheel 1 at measuring point 3 is 0.44. It can

be seen that the drive anti-skid control system has high reliability at low speed.

4.2   Medium speed group test

At a medium speed of 5-8 km/h, the slip rate without skid control function is shown in Figure 8a. All four wheels show obvious skid phenomenon, especially wheel 1 and wheel 4. As shown in Figure 8b after the drive anti-skid control system is opened, the slip rate data at all test points show that there is no slip phenomenon, and the average slip rate is about 0.03, which further verifies the reliability of the drive anti-skid control system.

4.3   High-speed group test

In the high-speed driving state of 12-15 km/h, the slip rate without the anti-skid control function is shown in Figure 9a, which may be due to the large ground unevenness, which makes it more difficult for wheels to maintain stable walking attitude and causes obvious yaw and roll.

As shown in Figure 9b after the drive anti-skid control system is opened, No. 2 test point on no. 3 driving wheel appears to slip, with a slip rate of 0.051, which exceeds the slip standard of 0.001. A review of high-speed photographic footage showed no slippage.

4.4   12-25 km/h speed reference group

As shown in Figure 10, the slip rate of the speed group is directly pushed to the limit speed from high-speed operation. When
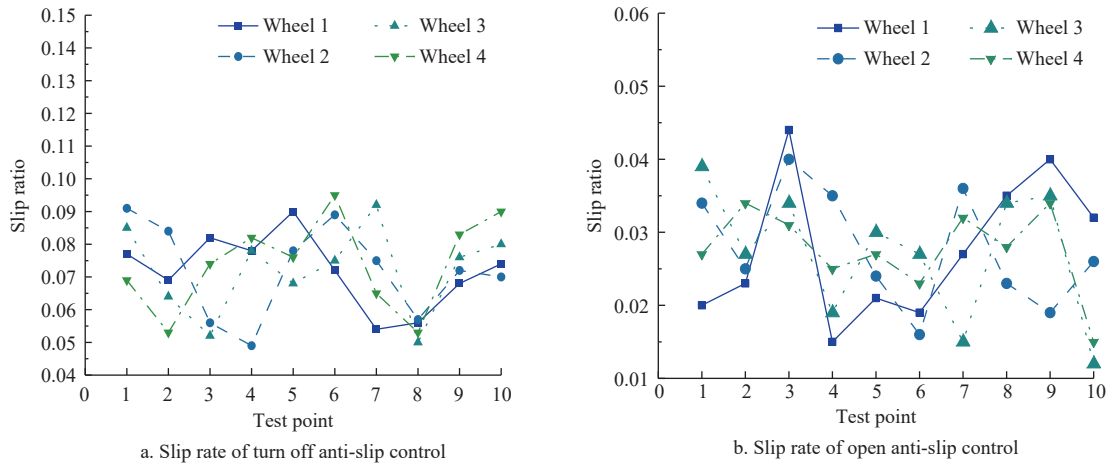
a. Slip rate of turn off anti-slip control   b. Slip rate of open anti-slip control

Figure 7   3-6 km/h comparison diagram of drive slip rate

a. Slip rate of turn off anti-slip control   b. Slip rate of open anti-slip control
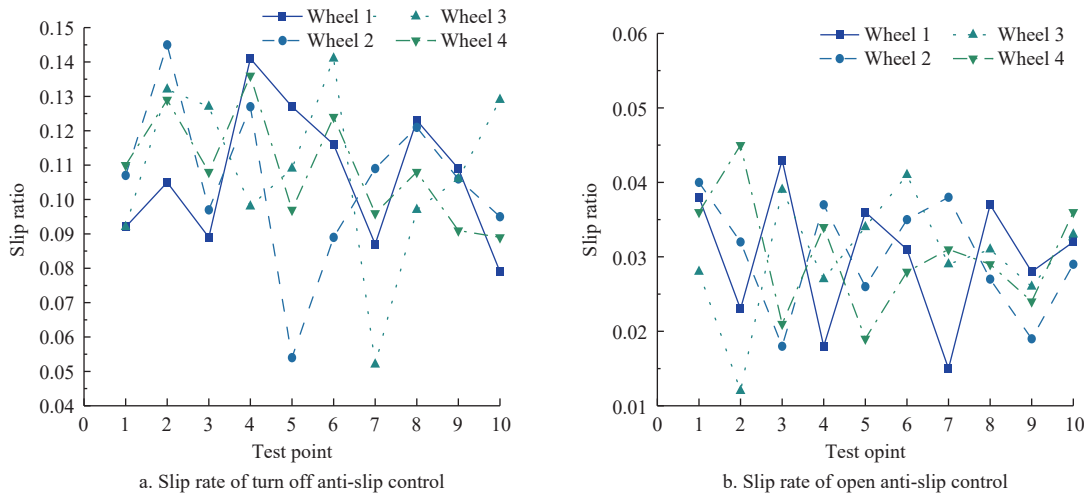
Figure 8   8-12 km/h comparison diagram of drive slip rate

a. Slip rate of turn-off anti-slip control   b. Slip rate of open anti-slip control
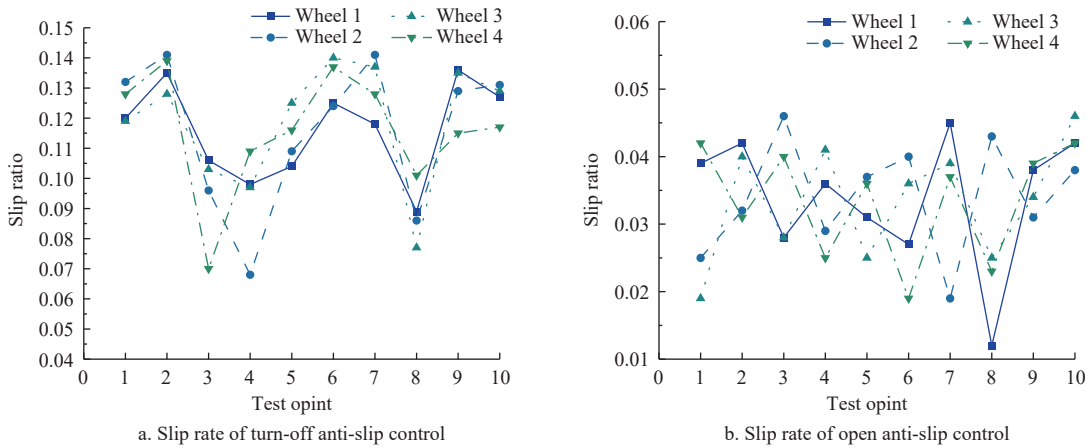
Figure 9   12-15 km/h Comparison diagram of drive slip rate

the anti-skid system is not started, there is a risk of falling on the test platform, which is for reference only. At test point two, wheel three slipped. Test point 9 skidded on wheel 4. The slip rate is 0.051.

4.5 Control system temperature, pressure feedback results

As shown in Figure 11, the rationality of the hydraulic system design was verified through the test results, and the main technical performance and key parameters of the system were obtained through the tests. The test results show that the hydraulic system design is reasonable and reliable, the system's high and low-speed switching, parking brake, service braking, anti-skid, emergency braking, brake release in emergencies, etc. are all normal. The main

technical performance of the system is consistent with the theoretical design requirements, such as the system main pressure of up to 380 bar and the system charge pressure of 24.00 bar The flushing flow of the flushing valve is 9-12 L/min, and the maximum driving speed is 25 km/h. All key parameters are within a reasonable range. For example, the pressure of the suction line of the plunger pump during cold start is −0.06 bar, the plunger The maximum casing pressure of the pump is 0.60 bar, which meets the requirements of the plunger pump used; the maximum drain pressure of the motor casing under hot operation is 4.00 bar, which meets the requirements of the motor used; at the same time, the
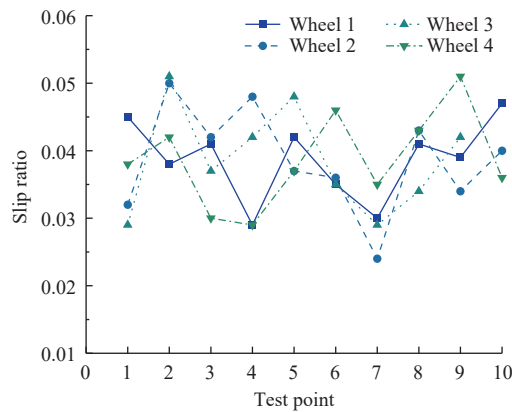
Figure 10   12-25 km/h anti-slip control diagram

hydraulic system has sufficient heat dissipation capacity. The test results show that after the thermal equilibrium is reached, the temperature of the hydraulic oil in the tank is about 44.4°C, the oil temperature in the mainline is 46.7°C, the oil temperature in the main pump drain port is about 55.1°C and the oil temperature in the motor casing drain port. Approximately 43.4°C, all lower than the temperature allowed by the hydraulic components and pipes. At the same time, the temperature difference between the hydraulic oil at the two ends of the radiator inlet and outlet is 6.2°C, and the radiator has sufficient heat dissipation capacity. The above results show that even when the ambient temperature is 40.0°C The temperature of the hydraulic oil in the system can also be stabilized below the maximum temperature allowed by the hydraulic system.

a. Measurement point temperature data diagram

b. Measurement point pressure data diagram

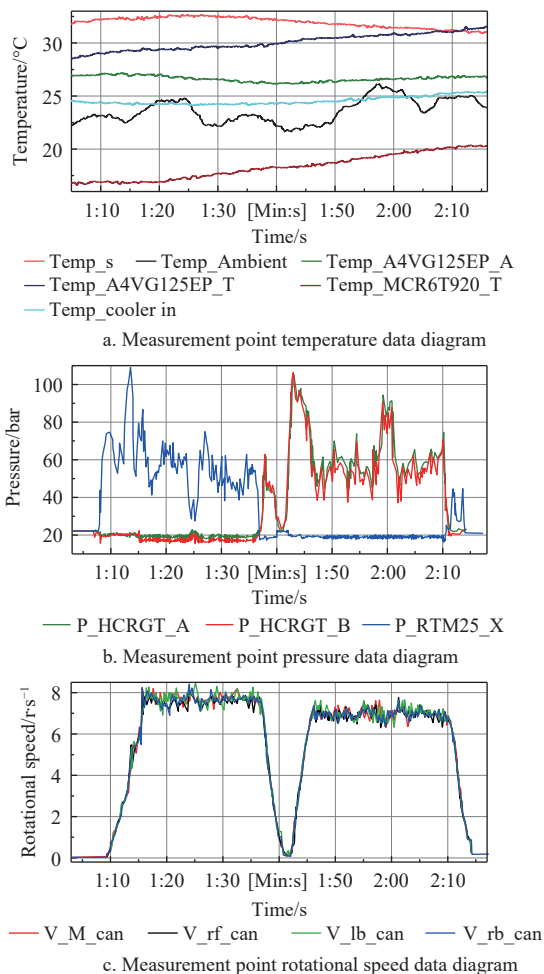c. Measurement point rotational speed data diagram

Figure 11   Test results of chassis-driven hydraulic system of self-propelled sprayer

5   Conclusions

Field experiments were carried out by the self-propelled non-skid control system of the self-propelled sprayer for high-stalk crops, based on the analysis of 280 sets of data obtained from the experiment (The slip rate of 160 groups of data for which the anti-slip control function is enabled and 120 groups of data for which the anti-slip control function is not enabled), the following conclusions are drawn:

In the data with the anti-skid control turned off, the slip rate was as high as 86.7%. In the data with the skid control turned on, according to the judgment condition of the slip rate of the mathematical model of 0.050, there were two groups exceeding this condition and both were 0.051, accounting for 1.25% of the total data.

The maximum main pressure of the Self-propelled sprayer for a high-stalk crops system is 380 bar, the system oil refill pressure is 24 bar, the flushing flow of the flushing valve is 9-12 L/min, and the maximum speed is 25 km/h. From the hydraulic test results, the following conclusions can be obtained:

1) The maximum drain pressure of the motor housing under hot operation is 4 bar, which meets the requirements of the motor used. After the heat balance is reached, the temperature of hydraulic oil in the tank is about 44.4°C, the oil temperature in the main circuit is 46.7°C, the oil temperature at the drain port of the main pump is about 55.1°C, and the oil temperature at the drain port of the motor shell is about 43.4°C, which are all lower than the temperature allowed by the hydraulic components and pipelines. At the same time, the temperature difference between the hydraulic oil at both ends of the oil inlet and outlet of the radiator is 6.2°C, and the heat dissipation capacity of the radiator is sufficient.

2) Through the comprehensive analysis of the field test and hydraulic test, the mathematical model of this study is accurate, the test results are within the error range, and all the work indicators meet the working requirements. Therefore, the self-propelled high-stalk crop sprayer drive system anti-slip control system can meet the needs of preventing the sprayer from slipping.

Acknowledgements

[References]

[1]   Yu J P. Development and application of plant protection machinery at home and abroad. Shangdong Agricultural Mechanization, 2020; 6: 28–31. (in Chinese)

[2]   Zhang C L, Li C P, Zhao C Z, Li L, Gao G L, Chen X Y. Design of hydrostatic chassis drive system for large plant protection machine. Agriculture, 2022; 12(8): 1118.

[3]   Lu L Q, Liu B, Mao E R, Song Z H, Chen J, Chen Y. Design and optimization of high ground clearance self-propelled sprayer chassis frame. Agriculture, 2023; 13(2): 233.

[4]   Zhang Z, Liu C G, Ma X J, Zhang Y Y, Chen L M. Driving force coordinated control of an 8×8 in-wheel motor drive vehicle with tire-road friction coefficient identification. Defence Technology, 2022; 18(1): 119–132.

[5]   Guo N Y, Zhang X D, Zou Y, Lenzo B, Zhang T, Gohlich D. A fast model predictive control allocation of distributed drive electric vehicles for tire slip energy saving with stability constraints. Control Engineering Practice, 2020; 102: 104554.

[6]   Fukui J, Miyazaki T. Speed control method for tilling claw of electric tiller

considering actual periodic reaction torque. IEEJ Journal of Industry Applications, 2019; 8(3): 539–547.

[7] Chen Q H. Study on anti-slip control for heavy-haul locomotives under complex wheel/rail friction conditions. Journal of Mechanical Engineering, 2023; 59(10): 179–186. (in Chinese)

[8] Chen L Q, Wang P P, Zhang P, Zheng Q, He J, Wang Q J. Performance analysis and test of a maize inter-row self-propelled thermal fogger chassis. Int J Agric & Biol Eng, 2018; 11(5): 100–107.

[9] Fu T. Research on driving anti-skid control technology of paddy field self-propelled sprayer. Master dissertation. Beijing: Chinese Academy of Agricultural Mechanization Science, 2018; 82p. (in Chinese)

[10] Liao Z L, Liu D, Yang G B, Chen L M. Integrated control of ABS and ASR for multi-wheel independent electric drive vehicle. Journal of Mechatronical & Electrical Engineering, 2018; 35(5): 494–500. (in Chinese)

[11] Guo H, Chen H F, Liu Q G, Xu Z Q, Gao G M, Xu X B. Design and research on hydraulic system of high gap wheel self-propelled sprayer. Journal of Agricultural Mechanization Research, 2018; 40(10): 51–56. (in Chinese)

[12] Liao Z L, Cai L C, Liu C G. Simulation research on anti-skid control electric vehicle driven by four wheel independent drive. Modern Information Technology, 2018; 2(2): 41–43. (in Chinese)

[13] Gao X, Guo J, Zhu Z, Han S. Design of power transmission system of high-clearance self-propelled sprayer. Journal of Agricultural Mechanization Research, 2017; 39(4): 247–251, 268. (in Chinese)

[14] Zhang H, Zheng J Q. Position control of electro-hydraulic actuator system for flexible sprayer chassis using fuzzy PID controller. Journal of Nanjing Forestry University (Natural Sciences Edition), 2017; 41(1): 163–169. (in Chinese)

[15] Wu N N. Research on structural analysis and dynamic simulation of a new type of differential. Master dissertation. Taiyuan: Taiyuan University of Science and Technology, 2013; 73p. (in Chinese)

[16] Ding L. Highland gap sprayer walking hydraulic drive system design

research. Master dissertation. Shihezi: Shihezi University, 2016; 81p. (in Chinese)

[17] Yu Z P, Wang Y B, Xiong L, Leng B. Analysis of the effect of anti-skid control of distributed-drive electric bus. Automotive Technology, 2016; 3: 18–25.

[18] Li G X, Ren Z Q. Design and test of voltage stabilization for sprayer spray system. Xinjiang Agricultural Mechanization, 2016(1): 21–22, 27.

[19] Wu Z B, Xie ., Chi R J, Yue F, Mao E R. Active modulation of torque distribution for dual-motor front- and rear-axle drive type electric vehicle based on slip ratio. Transactions of the CSAE, 2018; 34(15): 66–76. (in Chinese)

[20] Wang S T, Zhang X, Xie Z, Zhang X. Research on anti-skid control of wheel-driven electric vehicles based on road recognition. China Automobile Engineering Society. 2015 China Automobile Engineering Society Annual Meeting Proceedings (Volume1). China Automotive Engineering Society: China Automotive Engineering Society, 2015; pp.149–153.

[21] Wang J, He R. Hydraulic anti-lock braking control strategy of a vehicle based on a modified optimal sliding mode control method. Proceedings of the Institution of Mechanical Engineers, Part D: Journal of Automobile Engineering, 2019; 233(12): 3185–3198.

[22] Cao H F, Zhou J, Chen W, Lin Y, Li H P. Research on anti-sliding test method based on simulation technology. Railway Locomotives & Car, 2015; 35(3): 11–16. (in Chinese)

[23] Feng Y B, Yang J, Ji Z Y, Zhang W M. Fuzzy anti-slip control based on optimal slip control. Transactions of CSAE, 2015; 31(8): 119–125. (in Chinese)

[24] Li X W, Li Q A. Steering skid control system of high ground clearance hydraulic four-wheel drive sprayer. Science & Technology and Enterprise, 2015; 2: 254. (in Chinese)

[25] Song B T. Research on acceleration slip regulation control strategy of dual-motor four-wheel drive electric vehicle. Master dissertation. Zibo: Shandong University of Technology, 2022; 74p. (in Chinese)